INCORPORATING PERFORMANCE PREDICTION UNCERTAINTY INTO DETECTION AND TRACKING

21 February 2006

Lawrence D. Stone, Bryan R. Osborn
Metron Inc
11911 Freedom Drive, Suite 800
Reston, VA 20190

Robert T. Miyamoto, Chris Eggen, Marc Stewart, Andrew A. Ganse
Applied Physics Laboratory
University of Washington
1013 NE 40th Street
Seattle, WA 98105

Brian R. La Cour
Applied Research Laboratories
The University of Texas at Austin
P.O. Box 8029
Austin, TX 78713-8029

Daniel N. Fox
Rite Solutions
88 Silva Lane, Suite 220 East
Middletown, RI 02842

POC: Lawrence D. Stone, stone@metsci.com
703 787 8700 x440 (Ph) 703 787 3518 (Fax)

Short Title: Performance Prediction Uncertainty and Tracking

ABSTRACT

As part of the Uncertainty Directed Research Initiative of the Office of Naval Research, the authors have developed methods to characterize and quantify uncertainty in acoustic environmental predictions. We have developed methods for reflecting this uncertainty in tactical systems such as senor performance prediction, search plan recommendation, and track and detect systems that rely on environmental inputs. Uncertainty in performance prediction can result from model error and uncertainty in environmental information such as the bottom composition, sound speed profile, and background internal waves. In this paper, we characterize and quantify uncertainty in environmental predictions for the components of the sonar equation for multistatic active detection, and incorporate this uncertainty into a Bayesian track-before-detect system called the Likelihood Ratio Tracker (LRT). We present an example that applies LRT to multistatic active detection and tracking. For this example, we show that by incorporating environmental uncertainty into the LRT state space, we can make use of performance prediction while maintaining robustness to prediction errors.

I. INTRODUCTION

For many years the U.S. Navy has supported a vigorous program of collecting environmental data and developing models of the ocean environment. A major goal of this program is to provide environmental predictions that will allow the Navy to estimate detection performance for active and passive sonar systems used to detect submarines. These predictions are useful in optimizing sensor employment, planning searches, and performing tracking and detection functions. However, many times the uncertainties in these predictions prevent their effective use.

In 2001 the Office of Naval Research inaugurated the Capturing Uncertainty Directed Research Initiative (DRI). The goal of this DRI is to characterize and quantify the uncertainty in acoustic environmental predictions and to developed methods for reflecting this uncertainty in tactical systems such as sensor performance prediction systems that rely on environmental inputs. In this paper we describe the process that we have developed for quantifying uncertainty in environmental predictions. We then show how this uncertainty can be incorporated into a detection and tracking system in a way that allows us to use performance predictions while maintaining robustness to prediction errors.

Importance of Problem

The United States Navy is charged with the task of ensuring support for joint operations in support of United States national interests. A major component of supporting operations in foreign lands is to provide safe passage and areas of operation for ships at sea. Many foreign governments have turned to submarines as an effective weapon to defend their national interests. Highly capable submarines are easily obtained and can operate effectively beneath the ocean. This new generation of submarine threat is a serious challenge to U.S. supremacy at sea. The quiet diesel submarine, operating with modern technologies, can defeat most current United States ASW systems.

The extremely effective passive sonar systems, developed for the cold war, are not proving effective against these quieter, smaller diesel submarines. Active acoustic systems can provide a more reliable detection capability but make surface ships and submarines vulnerable to counter-detection. Air-deployed active multistatic sonobuoy systems, such as the Extended Echo Ranging (EER) system, provide active capabilities that can counter quiet diesel submarines, but they have had serious problems being introduced into the fleet.

An active sonar multistatic system, such as EER, must deal with two major issues: false targets and localization. False targets, arising from surface ships, bottom features, wrecks, and pipelines, are ubiquitous, consuming valuable operator time to validate each target-like echo and requiring more aircraft to validate contacts. Poor estimation of a target's position and path results in a large area of uncertainty. This consumes valuable resources (i.e., sonobuoy and aircraft time) to locate the suspected target and provide a definitive passive or non-acoustic classification for launching weapons. Therefore, failure to reduce false alarms and improve localization substantially degrades our operational capability

Dependence on Environment

While a system, such as EER, has been designed for single ping detection and localization, this hasn't proven to be a reliable capability. The Likelihood Ratio Tracker (LRT) described below is a Bayesian track-before-detect system that has been applied to EER. It is capable of integrating several below threshold responses over sensors and time to determine a detection and improve the detection and tracking performance of EER systems. LRT requires sensor performance predictions in order to calculate the likelihood functions used by the tracker. These performance predictions require good estimates of the environment. If these are correct, then they can enhance tracker performance. If the estimates are incorrect, they can degrade the performance of the tracker. By designing LRT to account for the uncertainty in performance prediction generated by uncertainty in the environmental predictions, we can obtain improved tracker performance while maintaining robustness to prediction error.

Motivation for Approach

While significant gains can be realized through the application of LRT to EER, providing accurate sensor performance prediction estimates is difficult. Sensor performance predictions are translated to LRT by using acoustic models to estimate signal excess (SE) on a target. Signal excess is the decibel level of a target's echo over a detection threshold above the background acoustic interference. While the actual acoustic interference (i.e., reverberation or noise) could be measured from the sensor system itself, sonobuoys are not calibrated and used in such a fashion. Rather, all components of the SE are calculated from acoustic models and their inputs. However, there are limitations on the accuracy of the acoustic modeling and their inputs. It is, in fact, impossible to reproduce nature precisely.

Definition of Uncertainty

We account for two types of uncertainty in this work, namely short term and model uncertainty. The short term uncertainty is caused by temporal fluctuations in the environment that occur over a period of minutes. These may be caused by internal waves for example. Model uncertainty is caused by our lack of knowledge of slowly varying or constant environmental parameters. For, example, we may have uncertain knowledge of the bottom type. This will produce uncertainty in predictions of propagations loss and signal excess. However, the bottom type will not change during the time that a buoy field is deployed. This long term uncertainty is called model uncertainty. It can also reflect errors in our acoustic models. We model both types of uncertainty through the use of probability distributions. We illustrate this by giving an example of short term and long term uncertainty models for signal excess prediction.

Uncertainty Models

We suppose there are a finite number of environmental models $\{E_1, E_2, \ldots, E_I\}$ that represent the environmental uncertainty in the region of interest. One of these models is the correct model for the area, but we are not sure which one it is. For each model we can compute an expected signal excess $\overline{SE}_i$ (in dB) for a specified source and receiver pair and target state (position and velocity). The actual signal excess (given model E_i is correct) is given by

$$\widehat{SE_i} = \overline{SE}_i + \xi$$

where ξ is a random variable with a specified distribution. For example, the distribution could be normal with mean 0 and specified standard deviation or it could have some other distribution such as a Rayleigh distribution. We assume that the value of ξ at time t is independent of the value at time $t+\delta$ where δ is the time between pings in a multistatic active situation. This represents the short term uncertainty in signal excess.

The long term or model uncertainty is represented by a discrete probability distribution on the finite set $\{E_1, E_2, \ldots, E_I\}$ of environmental models. This distribution is defined by

$$p_i = \Pr\{E_i \text{ is the correct model}\} \text{ for } i = 1, \ldots, I$$

and $\sum_{i=1}^{I} p_i = 1$.

Environmental Uncertainty

Environmental uncertainty arises from both incomplete knowledge of the environment and incomplete physics in the acoustic modeling. While models are not perfect, in general, most errors arise because of a lack of environmental characterization. As an example, the East China Sea (ECS) is an area that has one acoustic bottom loss versus bottom grazing angle function in the standard Navy database[1] for acoustic frequencies between 1000 and 10,000 Hz. The bottom loss function is a default value for all the world's oceans less than 200 meters and was meant to support a deep water sonar that bounced energy off the bottom to make a target contact. Direct measurements of the surficial sediments and acoustic measurements of propagation loss indicate that the standard Navy bottom is seriously in error. Moreover, the temperature and salinity from which sound speed is computed has substantial changes in time and space due to external mixing (winds) and pressure (tides), thus making an accurate estimate of the sound speed profile extremely difficult. Rather, an approach must be adopted that recognizes that there are inherent uncertainties in the estimation of the predicted acoustic environment that led to the acoustic detections that are actually seen.

Target Strength Uncertainty

Predictions of signal excess rely not only on environmental modeling but on modeling of the target as well. This adds an additional and important source of uncertainty for any active sonar processor which attempts to use modeled signal excess levels to compare with measured contact amplitudes. An obvious source of uncertainty is the choice of target submarine class to be hypothesized. Given the target identity, however, uncertainties will nevertheless arise from deficiencies in the target model. Much as in the case of environmental predictions, this may be due either to insufficient knowledge about the physical structure of the submarine in question or to intrinsic deficiencies in the scattering model. Finally, variability in time, say, from ping to ping, may arise due to changes in the target's kinematic state. In the LRT this kinematic state is the target's position and velocity, which are part of the hypothesized state variables of the tracker. Given this state, then, a prediction of target strength may be made based solely on the relative positions of the source, target, and receiver. The remaining variability may be modeled stochastically and arises physically from acoustic propagation effects coupled with an unknown target depth.

II. CHARACTERIZING ENVIRONMENTAL UNCERTAINTIES

Temperature Clustering

Traditional approaches to identifying representative sound speed profiles use historical (climatological) data sets grouped into months or seasons as well as geographical areas and then either average by depth or fit a representative curve. The Navy's official database is the Generalized Dynamic Environmental Model (GDEM) based on many years of data collections from different systems over most of the world. From that a variance about the nominal sound speed versus depth can provide an estimate of the uncertainty. However, the vertical structure of the water is not retained. To support tracking, it is important to retain the vertical structure of the water column that results in an acoustic field that governs detections. A new approach to identifying possible acoustic conditions is needed.

Raw historical profiles in an area can show considerable variability, but upon closer examination it is often the case that the profiles consist of a small number of modes, each of which consists of a family of similarly appearing profiles with a much smaller variability. In Fig. 1, the historical profiles in the East China Sea area are shown, along with a clustering which separates them into three internally similar subsets, each of which has significantly less variability than the original set. This allows us to represent the uncertainty in an area more accurately. For example, if we know that the water in the area on a given day is in mode 2, then we know from this analysis of historical profiles what the variability (uncertainty) will be. This, in turn, allows us to make a more accurate assessment of how this variability translates into uncertainty in the detection probability, for example.

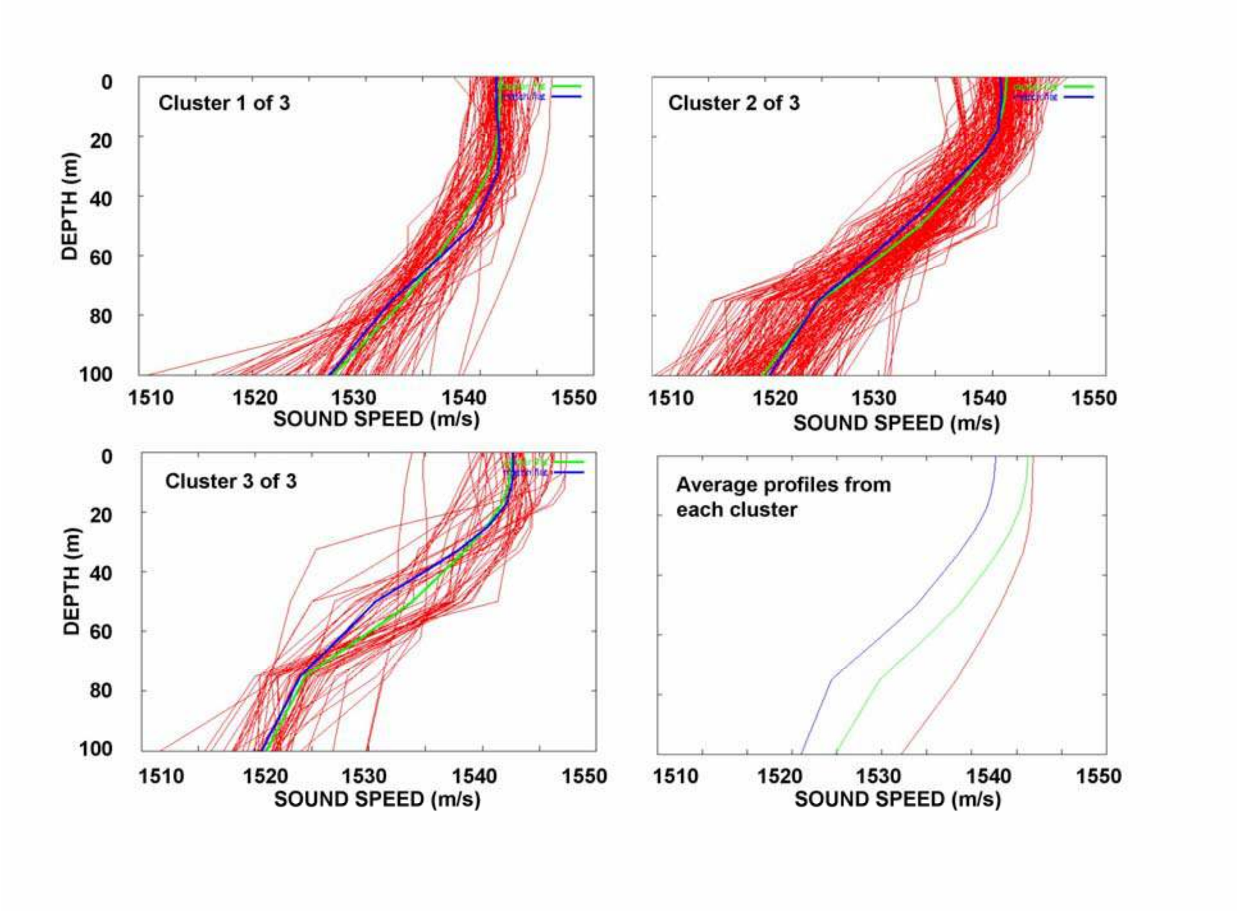

Figure1. Mean profiles for each of the four ECS sound speed clusters. The red lines in the cluster plots are historical measured sound speed profiles from the ECS taken over several years during the months of July to August. The green line within the cluster plot represents the average for each depth. The blue line represents a measured profile that is closest by Euclidean distance to the average profile. Finally, all three average profiles are shown.

It may be possible to determine the particular mode from remote sensing. The surface temperature and dynamic height of each profile can be related to a cluster. Satellite measurements of surface temperature and height (via altimetry) would indicate the most likely cluster, which would then allow us to estimate not only the profile shape but its uncertainty.

In cluster analysis, a series of 'attributes' is assigned to each datum, and the algorithm attempts to subdivide the dataset into subsets with similar attributes. In the case of profile data, we start with measurements of temperature (and possibly salinity) at arbitrary depths. This data is preprocessed to interpolate the measurements to fixed, standard depth levels. If measured salinities are not available, they are assigned using the database of historical T-S relationships available in the Modular Ocean Data Assimilation System (MODAS). The temperature and salinity measurements are then converted to sound speed, and additional attributes (such as the depth of the mixed layer, the sonic layer depth, and the near-surface vertical sound speed gradient) are computed.

There are three basic steps to clustering as applied here[2]. Cluster analysis uses similarity measures to group observations together. There are two parameters that must be defined in cluster analysis. First, a metric must be defined that quantifies profiles that are similar. This calculation is called the resemblance coefficient. A traditional metric is the Euclidian distance between two vectors and is used for our analysis. Specifically, the metric is the sum of the squared sound speed differences at the depths of 0.0, 2.5, 7.5, 12.5, 17.5, 25.0, 32.5, 40.0, 50.0, 62.5, 75.0, 100.0 meters. These specific depths are chosen since they are standard depths in oceanographic databases.

Second, the clustering method defines how the pairs of observations are grouped together based on their resemblance coefficients. Each cluster is defined as containing all observations whose resemblance coefficients are equal to within some tolerance. The clustering method starts by defining a tolerance such that each observation is in its own cluster. By repeatedly relaxing the tolerance, groups of similar observations fall into fewer and fewer clusters until finally all the observations are in a single cluster. Ward's Minimum Variance method[3] is used to cluster the sound speed data from the East China Sea.

Data for the cluster analysis on Sound Velocity Profile (SVP) data are calculated from temperature profiles taken during a Navy exercise, Ship Anti-submarine warfare Readiness and Effectiveness Measuring (SHAREM) 134, in the East China Sea. For this initial evaluation, data from all twelve months were processed from standard national ocean data archives. All the data was from regions of relatively shallow water. Only data with quality controlled, complete temperature profiles were used.

Lastly, once the clustering has been performed, the clustering tolerance is fixed to determine the similar observations. This choice defines the number of significant clusters and the observations that make up each cluster. Rather than setting the tolerance a priori, the data can be viewed at different tolerances and the clusters reviewed for the best groupings. For the ECS the four clusters were chosen to be representative. These clusters are shown in Fig. 1 along with the average profile for each cluster.

While there aren't dramatic differences in the ECS mean profiles, these are the likely states for acoustic propagation based on historical and in situ data. The impact of these profiles on the acoustic fields, including the impact of the bottom composition, will be discussed further in the section on propagation of uncertainty.

Bottom Characterization

Similar to the sound speed, the bottom composition needs to be characterized into possible conditions based on sources of error. These sources are the following: variations in measured grain size, variations in thickness of the sediment layer, and statistical uncertainty in the regressions relating grainsize to geoacoustic parameters such as sediment density, attenuation, scattering strength, and sound speed. The variability and uncertainty about means in these three sources propagate through the bottom model to create variability in the resulting bottom reflection loss (BL) and the bottom scattering strength (BSS) curve pairs. Realistic test distributions for each of these sources were modeled as Gaussian distributions derived from either the ASIA Experiment (ASIAEX)[13] measured data (for sediment thickness and measured grain sizes) or from regression statistics calculated from globally measured data (grain-size to geoacoustic-parameter relations).

The bottom acoustic model used in this analysis is a 2-layer analytic one developed by Darrell Jackson[11] of APL-UW. From 13 parameters of bottom properties such as density and sound speed in the two layers, as well as frequency and sound speed at the base of the water column, the model produces a curve pair of BL and BSS across the specified grazing angles. A Monte Carlo simulation with 1000 runs of the bottom acoustic model was set up to produce 1000 coupled BL and BSS curve pairs as shown in Fig. 2. Each run consisted of five sub-runs at frequencies from 150Hz to 1000Hz, for which the results were averaged together.

The resulting dataset of 1000 coupled BL and BSS curves serve as a PDF of loss and scattering for an area, which can be sampled for use in some broader ocean acoustic simulation. The complicated correlations between both the BL and BSS curves within a pair, as well as between each curves' values at different angles, made deriving some theoretical, continuous, joint PDF very daunting. However, by keeping a large enough dataset of BL and BSS curves, we inherently handle those complicated correlations. (For example, N = 1000 gives a margin of error of $1/\sqrt{N}$ which is equal to approximately 3% about the mean BL or BSS value at a given angle.)

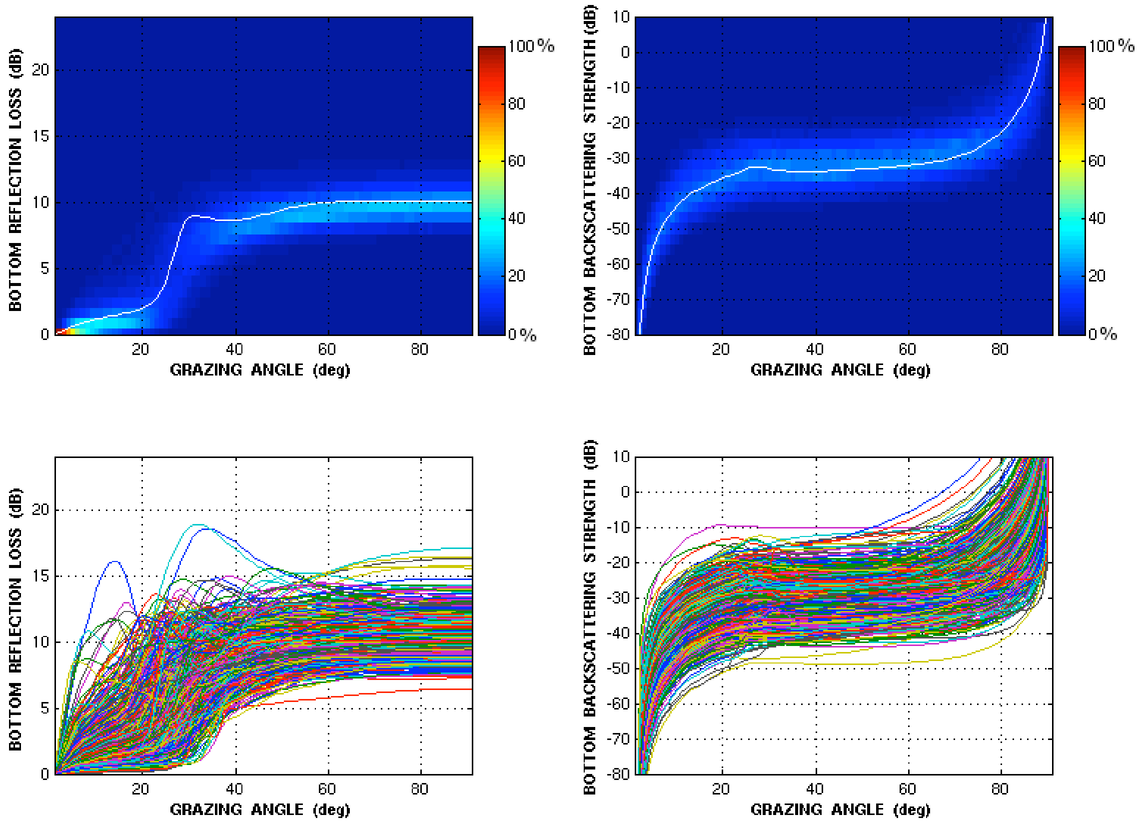

Figure 2. Bottom figures: all possible bottom loss and backscatter curves from 1000 realizations of possible geoacoustic bottoms for ECS. Top figures: color coded histogram of the most likely bottom loss and backscatter curves with white line overlay of the most likely condition

To simplify the calculation for the LRT simulation, four bottom types were selected from the distribution of possible sediment conditions. The four bottom types were selected by first averaging the bottom reflection loss and the bottom scattering strength for each realization over the range of grazing angles from 5 - 15 degrees which are the most important for shallow water acoustics. The median of the averaged curves was computed for the 1000 realizations. The median was used to separate the curves into high and low loss and scattering sets. Within the 500 low bottom reflection loss data set the median average bottom scattering strength was used as a threshold to further separate 500 realizations into a low bottom reflection loss data set, a low bottom scattering strength dataset, and a low bottom reflection loss with high bottom scattering strength subsets. Likewise, within the 500 high-BL data set, the median average BSS was used as a threshold to further separate 500 realizations into a high bottom reflection loss with low bottom scattering strength, and a (330) high bottom reflection loss with a high bottom backscatter strength subsets. For each subset a most likely bottom was found by computing a dB average and standard deviation of bottom reflection loss and scattering strength over all the realizations in the subset. Note that these are averages and standard deviations over a realization of data previously averaged over grazing angle intervals 5 - 15 deg. From each subset average we computed the root mean squared difference between the angle averaged bottom reflection loss and scattering strength for vectors in the subset and the means over the subset and then divide the average by the corresponding standard deviations to normalize the differences and sum the resulting normalized two curves. We ordered the difference sums to determine the highest and lowest differences and selected the smoothest curves. The final selection was made by human judgment. The four possible bottom types are shown in Fig. 3.

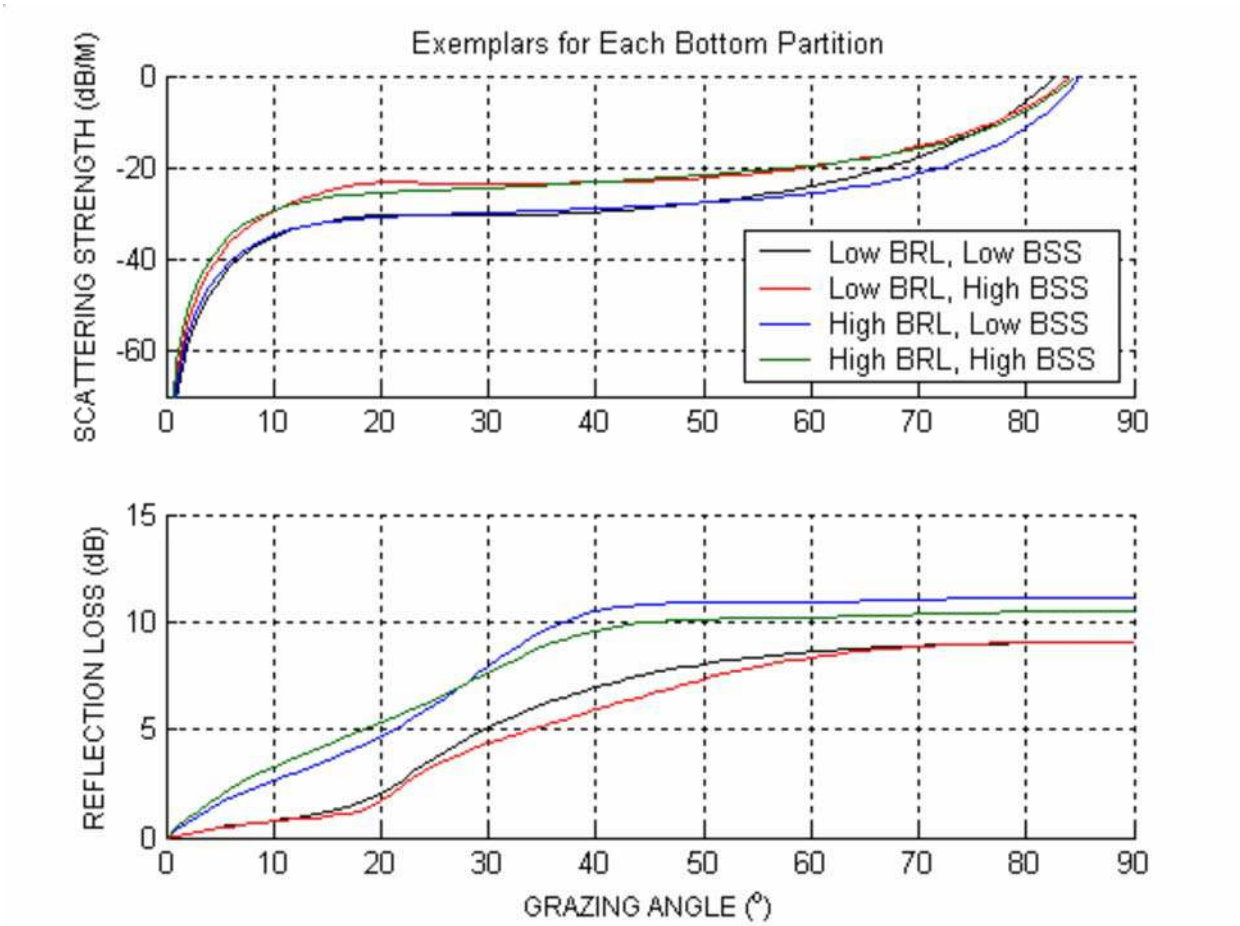

Figure 3. Resulting 4 possible bottom compositions that range from low bottom reflection loss with low bottom backscattering strength (black) to high bottom reflection loss with high bottom backscatter strength (green).

III. PROPAGATION OF UNCERTAINTY

The three possible sound speed conditions and the four possible bottom types are now considered the possible acoustic environments, and the Comprehensive Acoustic Sonar Simulation (CASS)[4] suite of software is used to calculate reverberation and transmission loss. In all of the modeling here, the propagation model was the Gaussian Ray Bundle (GRAB) approved as a standard Navy model. The resulting twelve different acoustic environments represent the uncertainty in the acoustic environments to be used by the tracker.

In order to provide suitable inputs for an active multistatic simulation, the reverberation needed to be calculated for bistatic geometries (separated source and receivers). For this simple case we kept a constant bottom depth of 100 meters and the climatological average wind speed of 8.8 meters/second. The bottom composition was assumed to be constant over the simulation area. The impulse source level was 245 dB for a 0.1 second pulse for a transmitter deployed at 30 meters depth. The receivers were also considered to be omni-directional at 10 meters depth. The frequency of all acoustic calculations was 750 Hz and was assumed to be constant over a band of 500 Hz.

The transmission loss calculation was modified from the conventional assumption of a continuous source to recognize that a short impulsive transmission would spread the energy in time due to multipaths. Therefore, the transmission loss calculation is the peak incoherent addition of all of the propagation paths to a fixed point in range and depth for a target depth of 50 meters.

Discussion of Acoustic Model Outputs

Since active multistatic systems have spatially separated sources and receivers, reverberation levels are calculated for discrete spacings in increments of 2.5 km. The resulting set of 12 reverberation curves is shown in Fig. 4. The peak bistatic reverberation levels drop off as the receiver separation increases; however, they tend to converge at later times. It is clear from the plots that the uncertainty in bottom reflection loss dominates the reverberation for ECS because of the many bottom interactions. A small uncertainty in bottom loss over many bounces is much more important than an uncertainty in the bottom backscatter strength or sound speed.

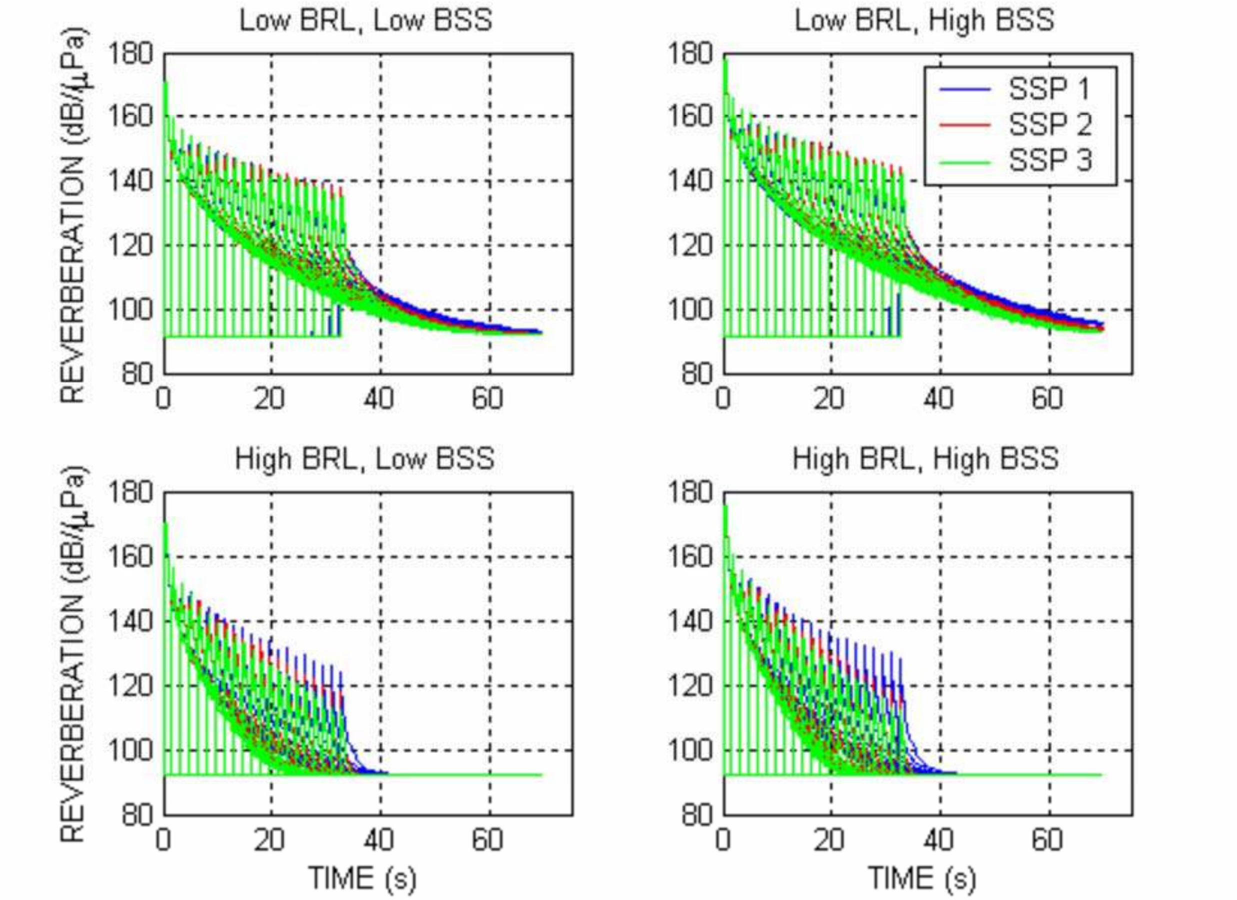

Figure 4. Monostatic and bistatic reverberation levels from CASS acoustic model using the four possible bottom compositions and the three possible sound speed profiles

A set of active acoustic TL calculations is shown in Fig. 5. These TL calculations show that the bottom reflection loss is the dominant factor in transmission loss over the range of possible sound speed conditions for this simulation. It is interesting to note that the high reflection loss bottom has a larger change in TL due to uncertainty in the sound speed. This is because there is a greater difference in bottom loss as the principal grazing angles to the bottom change due to the change in the sound speed profile. The light blue lines bracketing the dark blue line are one standard deviation above and below the mean transmission loss for SSP1. These are representative of the TL uncertainty. Since the mean TL curves for SSP2 and SSP3 fall outside of the TL uncertainty, it appears that our clustering provides significantly different environments.

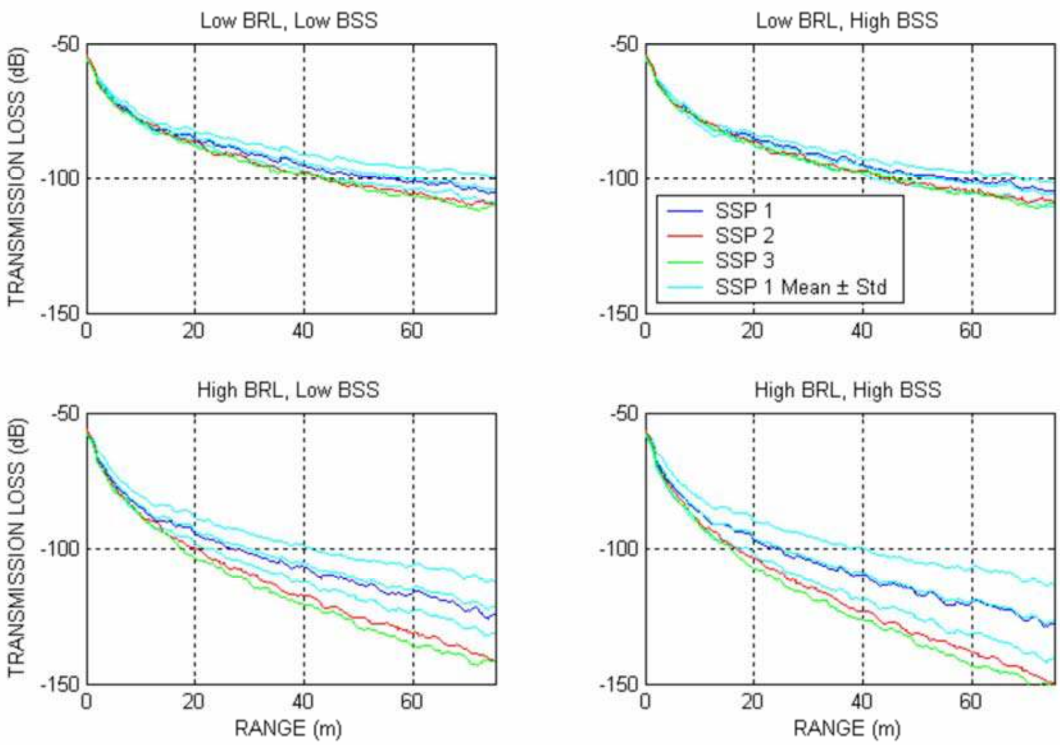

Figure 5. Transmission loss curves for the four possible bottom compositions and the three possible sound speed profiles as dark blue, red and green. The light blue curves are the mean plus or minus one standard deviation of the transmission loss resulting from the uncertainty in the sound speed for SSP1 from the clustering analysis

The acoustic model calculations provide the basis for the signal excess calculation. All of the system and environmental components are included. In order for the signal excess to be calculated all that remains is the target strength needed to calculate the target echo level.

IV. TARGET STRENGTH UNCERTAINTIES AND FLUCTUATIONS

Target strength (TS) is the component of the sonar equation which represents the response of a scatterer (i.e., a target submarine) to ensonification by an active source. Target strength is traditionally defined as the ratio of the intensity of the equivalent scattered plane wave to that of the incident plane wave[5]. Although the energy from such an interaction is always dispersed and attenuated, the target strength value itself is often over unity due to the fact that the incident intensity is measured at the acoustic scattering center, whereas the scattered intensity is measured with respect to a nonzero reference distance (usually 1 m) from this center. Defined as such, target strength is an inherently far-field, incoherent concept.

As a far-field quantity, target strength is in general a function of the source and receiver directions relative to the target. In addition, the target response to ensonification may be frequency dependent. Since target depth is generally not known or difficult to estimate, target strength predictions are often based on the assumption that both source and receiver are located in the horizontal plane of the target. At the mid-frequencies ranges typically used for active antisubmarine warfare (ASW), scattering is largely specular or ray-like and frequency dependence is slight.

Composite Target Modeling

A standard approach to computing target strength for complex objects is to treat the submarine as a composite of several more basic constituent objects, often referred to as *primitives*. Let $u(S,R,f)$ denote the total complex scattering function such that

$$\mathrm{TS}(S,R,f) = 20\log_{10}|u(S,R,f)|$$

is the target strength, in decibels, for a source at S ensonifying a target at frequency f and a receiver at R. Assuming linearity of the target response, the complex scattering function is a coherent sum of the individual complex scattering functions for each of the constituents. Thus, we may write

$$u(S,R,f) = \sum_n g_n(S,R,f)e^{j\delta_n(S,R,f)},$$

where $g_n(S,R,f)$ is the complex scattering function for the n^{th} constituent, situated at the origin, and $\delta_n(S,R,f)$ gives the phase delay due to the actual position of the object relative to the target origin.

To incorporate the broadband response of an active sonar transmission, one may integrate the product of the complex, frequency-dependent scattering function and transmit waveform spectrum over the frequency band to obtain an effective broadband target strength. Thus, the broadband target strength is given by

$$\mathrm{TS}(S,R) = 20 \log_{10} |u(S,R)|,$$

where

$$u(S,R) = \int u(S,R,f)\rho(f)df\,,$$

and $\rho(f)$ is the spectral density of the transmitted waveform.

In the high frequency regime where specular reflections dominate, R.E. Kell[6] showed in a classic result that a relationship exists between monostatic and bistatic radar cross-sections (RCS). This result translates directly in terms of target strength predictions and may be described as follows. Let $u_M(\theta,f)$ denote the monostatic scattering function at frequency f and angle θ, say, counter-clockwise from the target bow in horizontal plane. Let θ_S and θ_R denote the angles of the source and receiver. The bistatic theorem states that the bistatic scattering function, $u_B(\theta_S,\theta_R,f)$ may be written in terms of the monostatic scattering function as follows[7]

$$u_B(\theta_S,\theta_R,f) = u_M\left\{(\theta_S+\theta_R)/2, f\sec[(\theta_S-\theta_R)/2]\right\}.$$

This relationship is valid when the source and receiver directions are close to one another; i.e., when the bistatic angle, $\theta_S-\theta_R$, is small. Discrepancies between the true bistatic target strength and that predicted by the bistatic theorem may be attributed to wave effects, such as diffraction or the excitation of elastic waves, which become important at lower frequencies.

Target Strength Uncertainty

As discussed earlier, target strength is not a completely deterministic quantity, even when one is given the in-plane source and receiver directions relative to the target. A common approach to incorporating this additional element of uncertainty is to add to the scattering function a zero-mean random variable representing the short term, temporal variability of the measured target strength. We shall denote this random variable by $Z(\theta_S, \theta_R, f)$, recognizing that it general it may depend upon both the source/receiver directions as well as the frequency of ensonification.

A standard assumption is that $Z(\theta_S, \theta_R, f)$ is a complex Gaussian random variable with a mean of zero and a standard deviation $\sigma(\theta_S, \theta_R, f)$. The resulting magnitude of the total scattering function, $X = |u(\theta_S, \theta_R, f) + Z(\theta_S, \theta_R, f)|$, now has a Rician distribution. Let $f_X(x)$ be the probability density function (PDF) for X. Then

$$f_X(x) = \frac{2x}{\sigma^2} \exp\left(-\frac{x^2 + |u|^2}{\sigma^2} \right) I_0\left(\frac{2x|u|}{\sigma^2} \right) \text{ for } x \geq 0,$$

where $I_0(\cdot)$ is the zero-order modified Bessel function of the first kind, $\sigma = \sigma(\theta_S, \theta_R, f)$, and $u = u(\theta_S, \theta_R, f)$.

Written in terms of decibels, the target strength PDF is

$$f_Y(y) = \frac{\log 10}{20} 10^{y/20} f_X(10^{y/20}),$$

where $Y = 20\log_{10}(X)$. Sample plots of this distribution are shown in Fig. 6. It may be shown that the expectation of Y is given by

$$E(Y) = 20\log_{10}(u) + \frac{10}{\log 10}\Gamma(0, u^2/\sigma^2),$$

where $\Gamma(a,z)$ is the incomplete gamma function. For large SNR values, this expression is approximately equal to $10\log_{10}(u^2 + \sigma^2)$, the expectation of X^2 in decibels. Typical values for the standard deviation are on the order of 3 dB (i.e., $\sigma^2 = 2$).

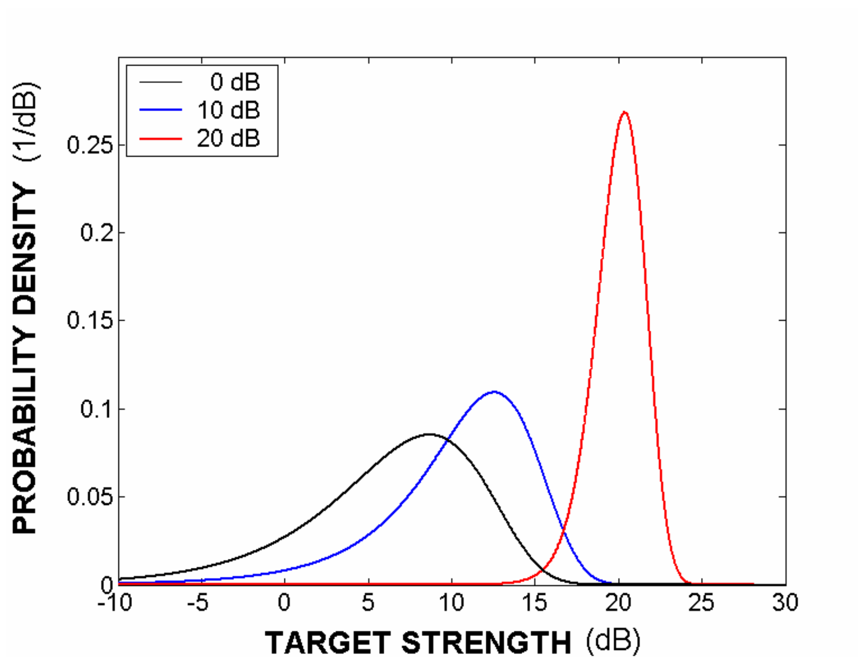

Figure 6: Plot of the target strength probability density function on a decibel scale. The three curves correspond to three different values of $20\log_{10}|u|$ with $\sigma = 1$. Note that for small signal-to-noise ratio (SNR), the distribution is highly skewed due to the nonlinear decibel scale. At larger SNR values the distribution becomes more Gaussian in shape.

Generic Diesel Electric Submarine

The target model used for the results discussed in this paper is the Bistatic Acoustic Simple Integrated Structure (BASIS) Target Strength Model developed by D. Drumheller at NRL-DC[8]. BASIS models targets as composites of simple geometric primitives whose individual responses are added coherently. The target strength predictions are fundamentally monostatic in that the bistatic theorem is used to determine bistatic target strength. Forward scattering is computed using Babinet's principle and each primitive's aspect-dependent cross section. For the results described in this paper, a model of a generic diesel electric submarine, 56 meters in length, provided in BASIS was used. The details of this model are provided in the above reference. Based on comparisons with finite element calculations, this model is expected to be valid for frequencies between 250 Hz and 2000 Hz.

For the present application, we considered the broadband target strength for a flat-spectrum waveform with a bandwidth of 500 Hz centered at 750 Hz. As was noted in the previous section, this frequency band is appropriate for an impulsive EER source. The broadband target strength was computed by coherently averaging the narrowband scattering function over a flat spectrum with frequency band 500-1000 Hz. In Fig 7, the results of the monostatic target strength calculations are shown and compared with predictions for 100 Hz and 0 Hz (narrowband) bandwidths. The values plotted are the expectation values for a constant σ of 3 dB. It may be noted that the variability of the target strength as a function of aspect angle tends to diminish as the bandwidth increases. This may be understood as a consequence of the coherent frequency averaging, whereby the detailed target responses at each frequency tends to be suppressed as they interfere with one another. The broad secondary peak appearing just above 90^{o} is due to the flat plane of the wedge used to model the sail. A more realistic, curved sail would suppress this peak.

The uncertainty in the target strength predictions is illustrated in Fig. 8. The figure shows the value of the target strength PDF for each aspect. For regions far off beam aspect (i.e., 90^{o}), where the target strength is low, the PDF is broad is heavily skewed toward lower values. By contrast, near the peaks in the monostatic target strength, the PDF is sharply peaked and nearly symmetric.

Finally, the broadband bistatic target strength, as computed from the bistatic theorem, is shown in Fig. 9. The monostatic prediction can be seen along the horizontal line at zero bistatic angle. The two ridges at bistatic aspect angles 90^{o} and 270^{o} correspond to specular reflections, where the angle of incidence from the source equals the angle of reflection to the receiver. The broad ridge at bistatic angle 180° corresponds to forward scattering, where the source, target, and receiver are collinear.

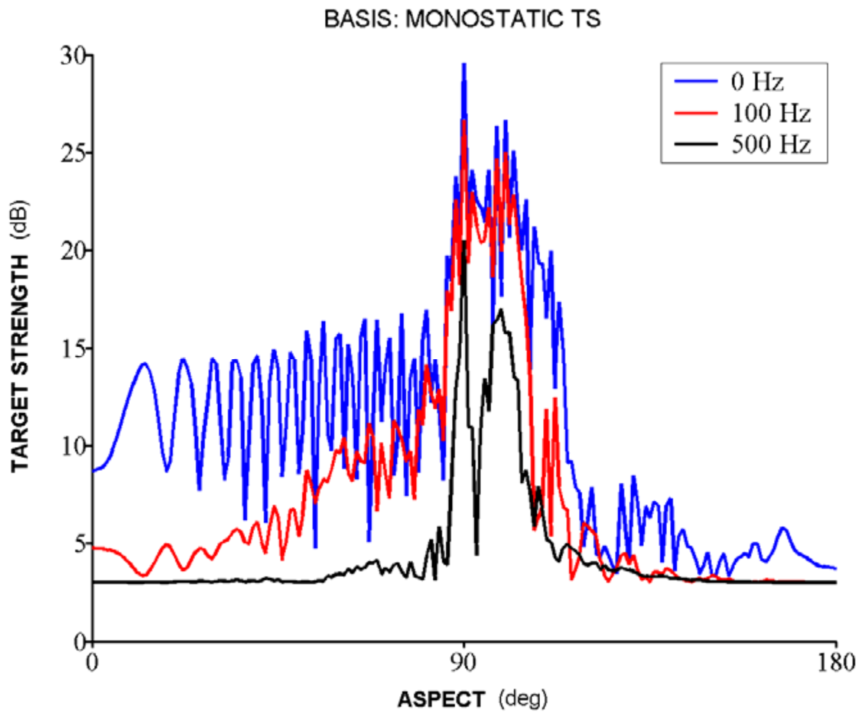

Figure 7. Plot of monostatic target strength for a generic diesel electric submarine modeled in BASIS. The values are the expected target strength for a constant standard deviation of 3 dB. The three overlays show the broadband target strength predictions for a pulse centered at 750 Hz with bandwidths of 0 (blue), 100 (red), and 500 (black) Hz. Due to the port-starboard symmetry of the target, only the target strength from bow to stern aspect is shown.

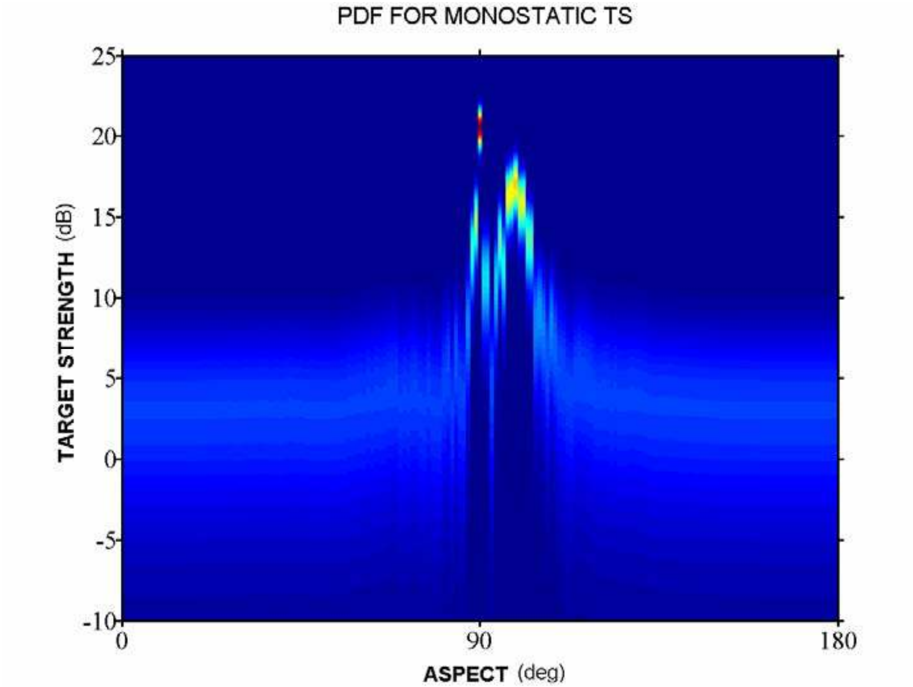

Figure 8. Plot of the broadband monostatic target strength PDF as a function of aspect, with each aspect corresponding to a separate PDF. The color indicates the value of the PDF for a given target strength and aspect, with blue indicating a low value and red indicating a high value.

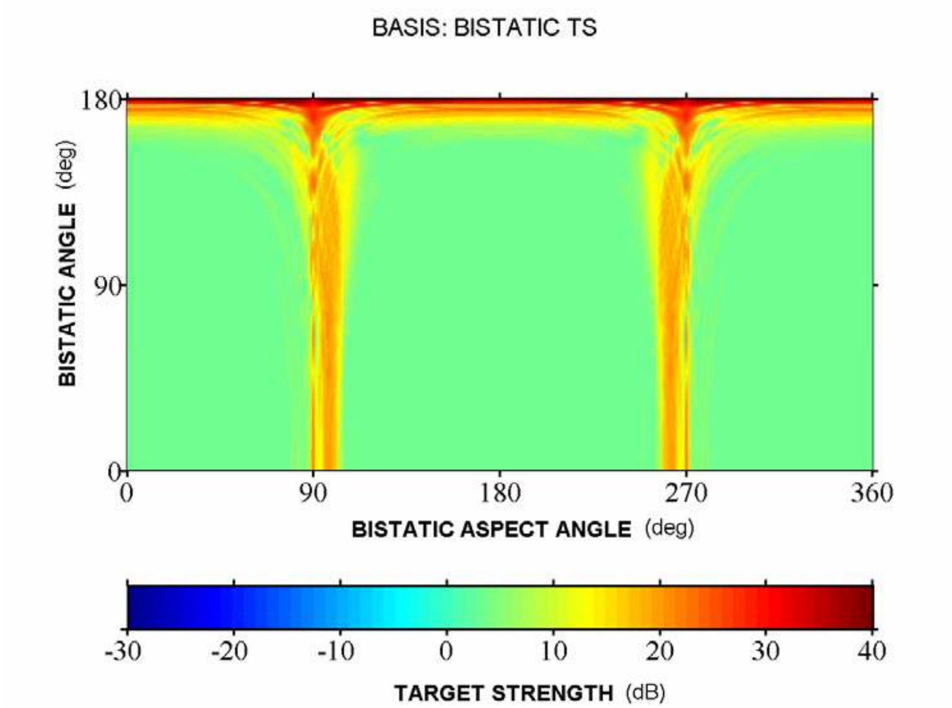

Figure 9. Plot of broadband bistatic target strength for generic diesel electric submarine model in BASIS. The color scale indicates the target strength in decibels. The horizontal axis is the bisector angle between the source and receiver directions. The vertical axis is the angular separation between these two directions.

For purposes of multistatic detection, it is important to note that most detections will tend to occur when the target is oriented with respect to the source and receiver such that a near specular reflection is provided. It is clear from the figure that most combinations of source and receiver directions will not provide a specular return, which creates a problem for bistatic detection. The forward scattering case, while providing a significant target strength value, may be difficult to utilize, as it may be difficult to distinguish from the direct blast. In the next section we will discuss a Bayesian approach to multistatic tracking which takes into account these subtleties by incorporating target strength predictions directly into the observation likelihood function.

V. LIKELIHOOD RATIO TRACKER

This section gives a brief description of the Likelihood Ratio Tracker (LRT) and discusses how we incorporated environmental uncertainty into LRT. Likelihood ratio (detection and) tracking is based on an extension of the single target tracking methodology to the case where there is either one or no target present. It is a Bayesian form of track-before-detect. LRT is designed for low Signal-to-Noise-Ratio (SNR) situations where several sensor responses must be integrated over time while the target is moving in order to call a detection. It is also appropriate for high false alarm situations such as those that arise in multistatic active systems that are operated with low contact thresholds. LRT's ability to integrate below-normal-detection-threshold data or even unthresholded data over space and time to detect weak targets allows it to produce improved detection performance without excessive false alarm rates.

Description of LRT

For LRT we identify a region $\mathcal{R}$ of interest. We let S be the target state space for a target in the region $\mathcal{R}$. Typically, S will the position and velocity of the target. If no target exists in $\mathcal{R}$, we shall formally refer to this state as the *null state* and designate it by the symbol ϕ. We augment the target state space S with this null state to make $S^{+} = S \cup \phi$. The augmented state space S^+ includes not only all of the states within $\mathcal{R}$ but the discrete null state ϕ as well. We shall assume there is a prior probability (density) function p_0 defined on S^+. Since we are assuming that there is at most one target in the region $\mathcal{R}$, we may write

$$p_0(\phi) + \int_{s\in S} p_0(s)ds = 1.$$

Let $X(t)$ be the (unknown) target state at time t. We start the problem at time 0 and are interested in estimating $X(t)$ for $t \geq 0$. The prior information about the target is represented by a Markov process $\{X(t); t \geq 0\}$. This process is specified by a prior probability distribution on the state of the target at time 0 and a Markov motion model that describes the target's motion through the state space S. There are one or more sensors that produce a set of K observations or measurements $\mathbf{Y}(t) = (Y_1, \ldots, Y_K)$ obtained in the time interval [0, t]. The observations are received at the discrete (possibly random) times $(t_1, \ldots, t_K)$ where $t_0 = 0 \leq t_1 \ldots \leq t_K \leq t$. From this information we can calculate the posterior state probability (density) in the standard Bayesian fashion[8].

$$p\left(t, s \mid \mathbf{Y}(t)\right) = \mathbf{Pr}\left\{X(t) = s \mid \mathbf{Y}(t)\right\} \text{ for } s \in S.$$

This is the posterior distribution on target state that is the standard output of a Bayesian tracker. We can also calculate the probability of receiving the sensor responses $\mathbf{Y}(t)$ given no target is present. This is

$$p\left(t, \phi \mid \mathbf{Y}(t)\right) = \mathbf{Pr}\left\{X(t) = \phi \mid \mathbf{Y}(t)\right\}.$$

We define the ratio of the posterior state probability (density) $p\left(t, s \mid \mathbf{Y}(t)\right)$ to the posterior null state probability $p\left(t, \phi \mid \mathbf{Y}(t)\right)$ as the *target likelihood ratio (density)* $\Lambda\left(t, s \mid \mathbf{Y}(t)\right)$; that is,

$$\Lambda\left(t, s \mid \mathbf{Y}(t)\right) = \frac{p\left(t, s \mid \mathbf{Y}(t)\right)}{p\left(t, \phi \mid \mathbf{Y}(t)\right)} \text{ for } s \in S. \tag{1}$$

At each time t, $\Lambda(t,\cdot \mid \mathbf{Y}(t))$ is a likelihood ratio surface defined over the state space S. Peaks in this surface indicate likely target locations. When the peak crosses a specified threshold, a detection is declared and the region near the peak is converted into a probability distribution for target state. This can be used to initiate a track on the target.

Target Motion

Target motion is modeled by a Markov process with transition function

$$q_k(s_k \mid s_{k-1}) = \mathbf{Pr}\left\{X(t_k) = s_k \,\middle|\, X(t_{k-1}) = s_{k-1}\right\} \text{ for } k \geq 1 .$$

Between the observation times, target motion is accounted for by applying this transition function to the target state distribution at time t_{k-1} to produce the projected target state distribution at time t_k as follows:

$$\begin{aligned} p^-\left(t_k, s \mid \mathbf{Y}(t_{k-1})\right) &= q_k(s \mid \phi) p\left(t_{k-1}, \phi \mid \mathbf{Y}(t_{k-1})\right) \\ &\quad + \int q_k(s \mid s_{k-1})\, p\left(t_{k-1}, s_{k-1} \mid \mathbf{Y}(t_{k-1})\right) ds_{k-1} \text{ for } s \in S. \end{aligned} \tag{2}$$

In the case of LRT, the state space includes ϕ, the target not present state, as well as the normal kinematic states. Thus we must specify the transition probabilities for leaving the region $\mathcal{R}$ as well as entering $\mathcal{R}$ from the state ϕ. Thus we may compute

$$\begin{aligned} p^-\left(t_k, \phi \mid \mathbf{Y}(t_{k-1})\right) &= q_k(\phi \mid \phi) p\left(t_{k-1}, \phi \mid \mathbf{Y}(t_{k-1})\right) \\ &\quad + \int_S q_k(\phi \mid s) p\left(t_{k-1}, s \mid \mathbf{Y}(t_{k-1})\right) ds. \end{aligned} \tag{3}$$

From (2) and (3) we can compute the motion updated likelihood ratio surface

$$\Lambda^-\left(t_k, s \mid \mathbf{Y}(t_{k-1})\right) = \frac{p^-\left(t_k, s \mid \mathbf{Y}(t_{k-1})\right)}{p^-\left(t_k, \phi \mid \mathbf{Y}(t_{k-1})\right)} \text{ for } s \in S . \tag{4}$$

The likelihood ratio density has the same dimensions as the state probability density. Furthermore, from the likelihood ratio density one may easily recover the state probability density as well as the probability of the null state.

Likelihood Functions

The sensor response or measurement $Y_k = y_k$ is incorporated into LRT through likelihood functions. Specifically,

$$L_k(y_k \mid s) = \mathbf{Pr}\{Y_k = y_k \mid X(t_k) = s\} \text{for } s \in S^+ .$$

Note that the data or observation $Y_k = y_k$ is known but the target state s is not. Thus the likelihood function $L_k(y_k \mid \cdot)$ is function of target state. Likelihood functions allow us to convert sensor responses or measurements of almost any kind into a common currency of information on the state space.

In LRT, we use the measurement likelihood ratio. It is the ratio of the likelihood of receiving the measurement given a target is present to the likelihood of receiving the measurement given no target is present. Specifically, we define the measurement likelihood ratio for $Y_k = y_k$ to be

$$\mathcal{L}_k(y_k \mid s) = \frac{L_k(y_k \mid s)}{L_k(y_k \mid \phi)} \quad \text{for } s \in S .$$

Likelihood ratio detection and tracking recursion

We can write a simplified recursion for likelihood ratio detection and tracking if we assume that

$$\begin{aligned} p^-(t_k, \phi \mid \mathbf{Y}(t_{k-1})) &= q_k(\phi \mid \phi) p(t_{k-1}, \phi \mid \mathbf{Y}(t_{k-1})) + \int_S q_k(\phi \mid s) p(t_{k-1}, s \mid \mathbf{Y}(t_{k-1})) ds \\ &= p(t_{k-1}, \phi \mid \mathbf{Y}(t_{k-1})). \end{aligned} \tag{5}$$

This assumption says that under the motion model, the amount of probability mass that moves out of the region $\mathcal{R}$ is equal to the amount that moves in for a given time period. Under this assumption we obtain the following likelihood ratio detection and tracking recursion.

Simplified Likelihood Ratio Detection and Tracking Recursion

Initialize Likelihood Ratio

$$\Lambda\left(0, s \,|\, \mathbf{Y}(0)\right) = \frac{p_0(s)}{p_0(\phi)} \text{ for } s \in S \qquad (6)$$

For $k \geq 1$ and $s \in S$

Motion Update

$$\Lambda^-\left(t_k, s \,|\, \mathbf{Y}(t_{k-1})\right) = q_k(s|\phi) + \int_S q_k(s \,|\, s_{k-1})\,\Lambda\left(t_{k-1}, s_{k-1} \,|\, \mathbf{Y}(t_{k-1})\right) ds_{k-1} \qquad (7)$$

Measurement Likelihood Ratio

$$\mathcal{L}_k\left(y_k \,|\, s\right) = \frac{L_k(y_k \,|\, s)}{L_k(y_k \,|\, \phi)} \text{ for } s \in S \qquad (8)$$

Information Update

$$\Lambda\left(t_k, s \,|\, \mathbf{Y}(t_k)\right) = \mathcal{L}_k\left(y_k \,|\, s\right)\Lambda^-\left(t_k, s \,|\, \mathbf{Y}(t_{k-1})\right) \text{ for } s \in S\,. \qquad (9)$$

Extension of LRT state space

Ordinarily LRT uses the target's kinematic variables for the tracker state space. For example, the state is often taken to be the target's 2 (or 3) dimensional position and velocity. For the analysis in this paper, we assume there are a finite number of possible environments with a prior distribution on which environment is the correct one. We extend the kinematic state space (2 dimensional position and velocity) to include environment. As sensor responses are obtained, LRT produces a joint estimate of target kinematic state and environment.

Numerical implementation of LRT

The implementation of LRT used to produce the results in the examples below employs a discrete grid in position, velocity, and environment. The methodology is similar to the gridded version of Nodestar described in Chapter 3 of Stone, Barlow, and Corwin[9].

Measurement Likelihood Ratio Function

The examples presented in this paper involve multi-static active (MSA) sonar. There are a set of 10 to 30 buoy pairs. Each pair consists of a receiver buoy and a source buoy with two explosive charges. These buoy pairs are distributed over an area where a target submarine may be present. The charges on the source buoys are detonated sequentially, one every few minutes. Between detonations, the hydrophones in the receiver buoys listen for echoes of the shockwave as it scatters off objects, potentially including a moving target submarine. The time between the reception of the direct blast and an echo produces an ellipse of possible locations for the echo producer. By accumulating a number of these echoes from the target, it is possible to call a detection and develop a track on the target, i.e., a distribution on the target's position and velocity.

The signal processing algorithms associated with these buoys are presumed to process the acoustic time-series at the receiver hydrophones and call detections. These algorithms produce a set of time values for each hydrophone where the signal or matched-filter output exceeds some threshold. Each of these "detections" comes from one of three things: random stochastic fluctuations in the noise signal (false alarms), clutter echo, or a target echo. These are the measurements used by LRT.

In some situations the Signal-to-Noise Ratio (SNR) at the receiving buoy is high enough that a bearing is also obtained. However, for the examples presented below, we assume that no bearing information is available.

Known Probability of Detection

To simplify our presentation, we first introduce the measurement likelihood ratio function for MSA sonar in the case where the detection probability is known. For a single ping, let $\boldsymbol{\tau}_l = \{\tau_1, \ldots, \tau_n\}$ be the set of echo times detected at buoy l. The measurement likelihood ratio for $\boldsymbol{\tau}_l$ is

$$\begin{aligned}\mathcal{L}_l(\boldsymbol{\tau}_l \mid s) &\equiv \frac{\mathbf{Pr}\{\text{Obtaining } \boldsymbol{\tau}_l \text{ at buoy } l \mid \text{target in state } s\}}{\mathbf{Pr}\{\text{Obtaining } \boldsymbol{\tau}_l \text{ at buoy } l \mid \text{no target present}\}} \\ &= P_d^{\,l}(s) \sum_{i=1}^{n} \frac{1}{\lambda} \left(\frac{f_l(\tau_i \mid s)}{w(\tau_i)} \right) + \left(1 - P_d^{\,l}(s)\right)\end{aligned} \tag{10}$$

where

$s =$ target state (x, v), position and velocity
$f_l(\tau \mid s) = \mathbf{Pr}\{\text{receiving an echo at buoy } l \text{ at time } \tau \mid \text{target detected in state } s\}$
$w(\tau) = \mathbf{Pr}\{\text{receiving an echo at time } \tau \mid \text{ echo generated by false alarm}\}$
The number of false alarms per ping per buoy is Poisson distributed with mean λ
$P_d^{\,l}(s) = \mathbf{Pr}\{\text{buoy } l \text{ detects a target in state } s \text{ on a single ping}\}$.

The derivation of (10) is given in the appendix of Stone and Osborn[10]. To form the composite measurement likelihood ratio function for a single ping, we multiply the measurement likelihood ratio function for each of the buoys as follows. Let $\boldsymbol{\tau} = (\boldsymbol{\tau}_1, \ldots, \boldsymbol{\tau}_{N_r})$. Then

$$\mathcal{L}_{\mathbf{C}}(\boldsymbol{\tau} \mid s) = \prod_{l=1}^{N_r} \mathcal{L}_l(\boldsymbol{\tau}_l \mid s) \tag{11}$$

where N_r is the number of receiver buoys. This measurement likelihood ratio is multiplied into the motion updated cumulative likelihood ratio to obtain the posterior cumulative likelihood ratio in the information update step in (9). This process is repeated for each ping.

The measurement density function $f_l(\tau\,|\,s)$ represents the "ellipse" information from the time of detection. Let x_s^m be the position of source m and x_r^l be the position of the receiver buoy l. Then the measurement error density function for the arrival time τ from source m is

$$f_l\left(\tau\,|\,s=(x,v)\right)=\frac{1}{\sqrt{2\pi}\sigma_t}\exp\left\{\frac{\left(c_s\tau-d(x_s^m,x)-d(x,x_r^l)\right)^2}{c_s^2 2\sigma_t^2}\right\} \tag{12}$$

where $d(x_1,x_2)$ is the distance between positions x_1 and x_2, and c_s is the sound speed. We use σ_t = 1 second. This form of the measurement error density function can also be used to account for uncertainty in buoy position to first order, as we have shown elsewhere. The false alarm density function w is uniform over a 90 second interval after the arrival of the direct blast.

The $P_d^{\,l}(s)$ factor is where we require a performance prediction model for the sensors, and this is where environmental information is incorporated into the LRT algorithm. To compute $P_d^{\,l}(s)$ for a given source m, we begin by computing the mean signal excess $\overline{SE}$ in dB at the receiver buoy l as follows.

$$\overline{SE}_{lm}(s)=SL_m-TL_m(s)+TS_{lm}(s)-TL_l(s)-(RL_{lm}(s)+AN)-DT \tag{13}$$

where

$SL_m =$ source level at source m
$TL_m(s) =$ transmission loss from source m to state s
$TS_{lm}(s) =$ target strength for a signal from source m reflected from a target in state s to sensor l
$TL_l(s) =$ transmission loss from state s to sensor l
$RL_{lm}(s) =$ reverberation at sensor l from source m at the time an echo arrives from state s
$AN =$ ambient noise level
$DT =$ detection threshold.

The value of $\overline{SE}_{lm}$ given by equation (13) represents the mean signal excess level. The actual value of signal excess $\widetilde{SE}$ is a random variable with fluctuations about this mean that are normally distributed with mean 0 and standard deviation σ_{SE} generally taken to be between 5 to

10 dB. Detection occurs when $\widetilde{SE} > 0$. Having calculated $\overline{SE_{lm}}(s)$ from (13), we can compute $P_d^{\,l}\left(s\right)$ as follows

$$P_d^{\,l}\left(s\right) = \int_0^{\infty} \eta(x, \overline{SE}(s), \sigma_{SE}^2)\, dx$$

where $\eta(\cdot, \mu, \sigma^2)$ is the density function for a normal distribution with mean μ and variance σ^2.

Incorporating Prediction Uncertainty

The procedure for computing the likelihood function described in the previous section assumes we know the terms in equation (13) with certainty. When there is uncertainty in these terms, we must modify our procedure. We account for this uncertainty by extending the LRT state space to include an "environmental-uncertainty" dimension where each value in this dimension represents one possible environment, E. The likelihood function then becomes

$$\mathcal{L}_l\left(\boldsymbol{\tau} \,|\, s, E\right) = P_d^{\,l}\left(s, E\right) \sum_{i=1}^{n} \frac{1}{\lambda} \left(\frac{f_l\left(\tau_i \,|\, s\right)}{w\left(\tau_i\right)} \right) + \left(1 - P_d^{\,l}\left(s, E\right)\right), \tag{14}$$

where we now have a likelihood function that is defined not only over the target's kinematic state space, but also over the extra environmental dimension. The values of $E \in \{E_1, E_2, \ldots\}$ represent all possible environments. For the examples that we consider below, each environment consists essentially of a reverberation and transmission loss characterization. Furthermore, as we are using range independent environments for this work, we have $RL \equiv RL(d,t)$ and $TL \equiv TL(d)$: reverberation is a function of the distance between source and receiver and time since blast while transmission loss is a function of distance only. Thus, $E_i \equiv \{RL^i, TL^i\}$. The Applied Research Laboratory, University of Texas, and the Applied Physics Laboratory at University of Washington have computed these functions for us from more basic environmental parameters such as bottom type and sound speed profiles appropriate for a specific ocean area.

VI. EXAMPLE

This section provides an example of using LRT with environmental prediction uncertainty incorporated by the method described above. For the example, we consider the East China Sea region described above and use the twelve environmental models selected to span the uncertainty in the East China Sea's bottom type and sound speed profile (SSP). Four representative bottom types are used with three representative SSPs to arrive at twelve distinct environments. Table 1 lists these environments along with their probabilities of representing the correct environment. Each of these twelve environments gives rise to its own mean reverberation and transmission loss estimates. The three SSPs are labeled 1, 2, 3. The bottom reflection loss (BL) and the bottom scattering strength (BSS) are labeled as H or L for high or low. Thus the environment designated 1/H:H has SSP 1, high BL, and high BSS.

Env #	*Designation*	*SSP*	*BL*	*BSS*	*Probability*
1	*1 / H:H*	*1*	*H*	*H*	*0.309 / 3.0*
2	*1 / H:L*	*1*	*H*	*L*	*0.191 / 3.0*
3	*1 / L:H*	*1*	*L*	*H*	*0.191 / 3.0*
4	*1 / L:L*	*1*	*L*	*L*	*0.309 / 3.0*
5	*2 / H:H*	*2*	*H*	*H*	*0.309 / 3.0*
6	*2 / H:L*	*2*	*H*	*L*	*0.191 / 3.0*
7	*2 / L:H*	*2*	*L*	*H*	*0.191 / 3.0*
8	*2 / L:L*	*2*	*L*	*L*	*0.309 / 3.0*
9	*3 / H:H*	*3*	*H*	*H*	*0.309 / 3.0*
10	*3 / H:L*	*3*	*H*	*L*	*0.191 / 3.0*
11	*3 / L:H*	*3*	*L*	*H*	*0.191 / 3.0*
12	*3 / L:L*	*3*	*L*	*L*	*0.309 / 3.0*

Table 1. Summary of the twelve environmental models. Each of the twelve environments is a combination of an SSP, BL, and BSS. Each SSP has an equal probability of occurrence. The BL/BSS combinations of H/H and L/L have a probability of 0.309 while the H/L and L/H combinations have a probability of .191.

In what follows, we apply the likelihood ratio tracker described in the previous sections to a set of simulated EER detection data. We show that the tracker successfully detects the target in the presence of the environmental uncertainty and that the marginal likelihood on environment peaks on the correct environment. We also show that if we had picked a single incorrect environment and run LRT using only that environment, the tracker would have failed to detect the target.

Description of Simulation

We simulated a set of EER detections to use as input measurements to the tracker. Below we describe how we simulated target detections and false alarms as well as how the measurement likelihood ratio is computed from these inputs. We also describe the layout of the buoy field, the target's actual track, and the parameters used by the tracker.

Simulating Detections

To produce simulated target detections we used environment 2/L:L to compute reverberation and transmission loss for the modeled detection data. Thus this environment is true environment for this example. For each ping we used equation (13) to determine the mean signal excess for each buoy l in the field. Each of the terms in equation (13) were determined as follows where m is the index of the source buoy for the ping:

$SL_m = 245$ dB
$s =$ target's state (position and velocity) in the simulation at the time of the ping
$TL_m(s)$ and $TL_l(s)$ are computed using envrionment 2/L:L
$TS_{lm}(s)$ is computed using the Basis bistatic target strength model for a small Diesel
$RL_{lm}(s)$ is computed using envrionment 2/L:L
$AN = 92$ dB
$DT = 3$ dB.

Equation (13) is used to compute $\overline{SE}_{lm}(s)$. For each receiver buoy, we make an independent draw from a Gaussian distribution with mean 0 and standard deviation 5 dB to obtain ξ_{lm}. A simulated detection occurs at buoy l if $\overline{SE}_{lm}(s) + \xi_{lm} > 0$. If this happens, then we make a draw from a distribution which is Gaussian with mean $\left[d(x_s^m, x(s)) + d(x(s), x_r^l)\right]/c_s$ and standard deviation 1 second to determine the echo time for this detection where $x(s)$ is the position of the target at the time of the ping.

For each ping and each receiver buoy, the number of false alarms is determine by an independent draw from a Poisson distribution with a mean of ten. The times of the false alarm detections are independently and uniformly distributed over the 90 second dwell period following the reception of the direct blast.

For each buoy l and ping, the set of times comprising the echo time of the target detection (if detection occurs) plus the false alarm detection times is the measurement vector $\boldsymbol{\tau}_l$. Let $\boldsymbol{\tau} = (\boldsymbol{\tau}_1, \ldots, \boldsymbol{\tau}_{N_r})$ be the vector of measurements from all the buoys. This measurement vector is used to compute the composite likelihood ratio function in (14) for each environment. Note, for this computation we have to compute $P_d^{\,l}\left(s, E\right)$ for each of the 12 environments $E = E_i$ for $i = 1, \ldots, 12$ and each target state s for each buoy.

As a way of seeing the differences in expected signal excess predictions produced by the different environments, we show monostatic mean signal excess predictions as a function of range for each environment in Figs. 10 and 11. Note the monostatic predictions involve only one way transmission loss and do not incorporate target strength.

Kinematic Assumptions

The simulation uses a 30 km by 30 km regularly spaced rectangular grid of 25 buoys. These buoys ping twice each in a random order with three minutes between pings and a 90 second dwell time. The target moves with constant velocity at 4 m/s from the south-west corner of the buoy field directly toward the north-east corner of the buoy field.

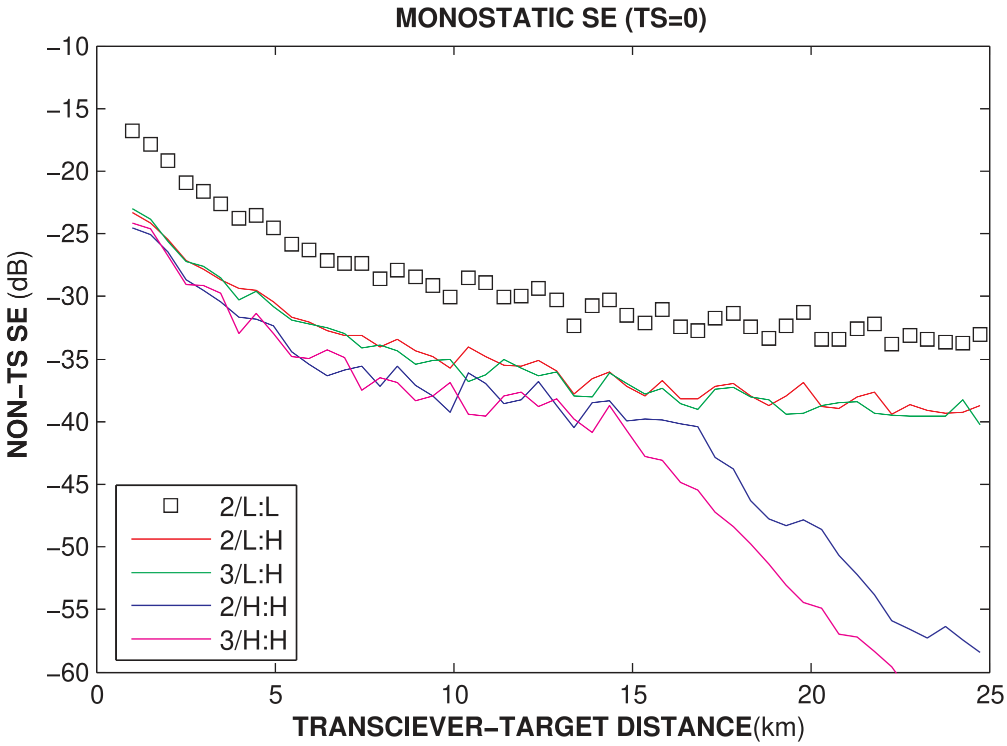

Figure 10. Monostatic SE for environments which produce substantially different monostatic SE from environment 2/L:L. These values reflect source level, reverberation, transmission loss, and ambient noise signal excess components.

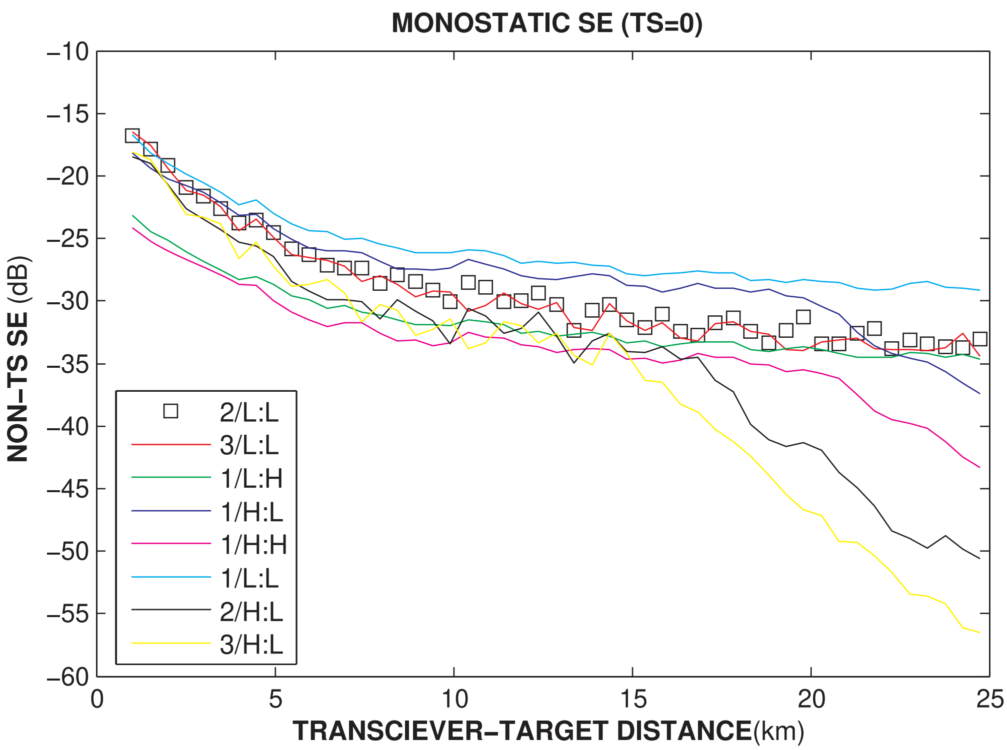

Figure 11. Monostatic SE for environments which produce monostatic SE similar to environment 2/L:L. These values reflect source level, reverberation, transmission loss, and ambient noise signal excess components.

Likelihood Ratio Tracker Parameters

To process the detection data we use the likelihood ratio tracking technique detailed in the previous sections. A set of 200 velocity hypotheses are used. These are uniformly spaced in the annulus of velocities defined by headings in the range from 0 to 360 degrees and speeds from 1 to 8 meters per second. The spatial domain is divided into a set of 750 m by 750 m cells and covers an area 70 km by 70 km. The prior distribution is weighted according to the probability of occurrence of each of the twelve environments but is uniform over space and velocity. The initial distribution on environment is independent of target state. We use a motion model whereby the target chooses a new course and speed from the above velocity distribution at time intervals having an exponential distribution with mean 30 minutes.

Description of Results

The results of processing the simulated EER detection data with the Likelihood Ratio Tracker show that the target is detected and that the likelihood peak appears on the correct environment. We also note that some of the environments that are significantly different from 2/L:L do not show any peak on the target.

Figure 12 shows the maximum cumulative log likelihood ratio at 2:03 over all velocities and environments as a function of position. Note that there is a strong likelihood peak on the target, indicating that the target would have been successfully detected. Figure 13 shows the maximum cumulative log likelihood ratio at 2:03 over all velocities as a function of position. conditioned on the 2/L:L, environment, which is the environment used by the simulation. Again we see the likelihood peak is on the target. Figure 14 shows the maximum cumulative log likelihood ratio at 2:03 over all velocities as a function of position conditioned on one of the incorrect environments. Note that the peak log likelihood ratio is much lower and not localized near the target. This suggests that had this incorrect environment been used for the tracker, the operator may have failed to detect the target.

Figure 15 shows a plot of the maximum log likelihood ratio at time 2:03 for all environments. The reader will note that the 2/L:L environment has the highest value, but some other environments also had maximum values that are nearly the same the 2/L:L environment. However, by comparing this figure with Fig. 11, the reader can see that these environments look very similar in their monostatic SE to the correct 2/L:L environment. In addition from Figs. 10 and 15, one can see that the environments with the lowest maximum likelihood ratio are those that appear most different from environment 2/L:L in their monostatic SE.

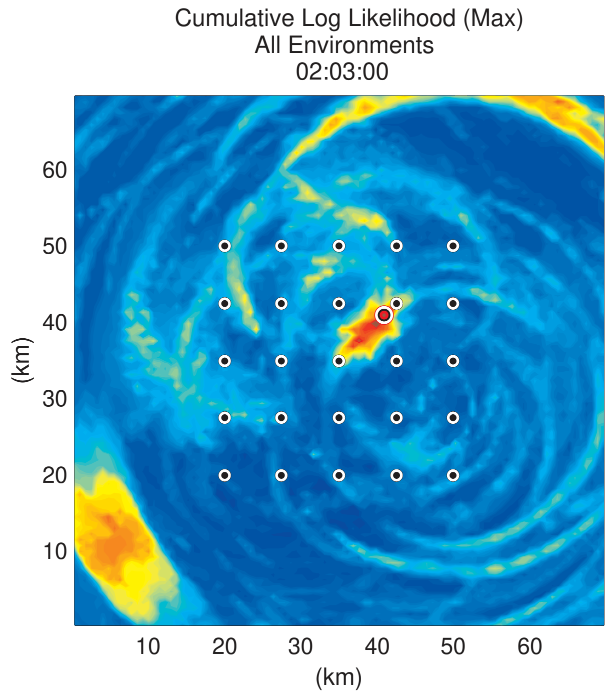

Figure 12. Maximum cumulative log likelihood ratio at 2:03 as a function of position for the all environments case. For each position state, the figure shows the maximum of the cumulative log likelihood ratios over all environments and velocities for that position.

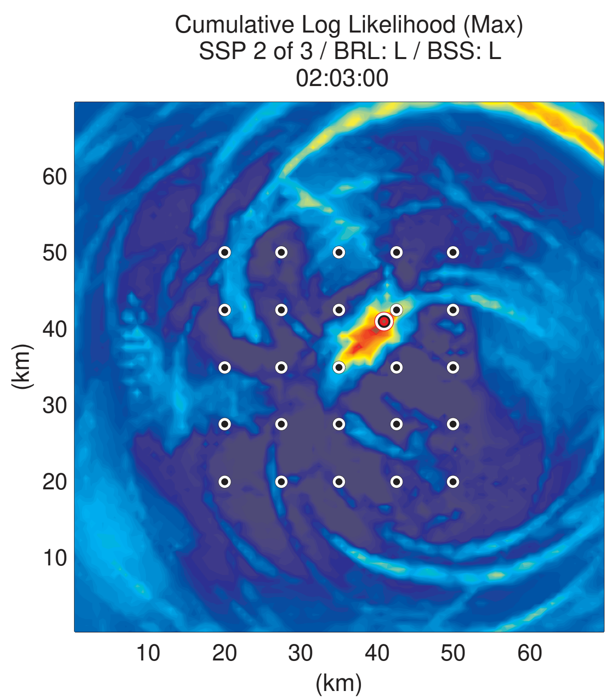

Figure 13. Maximum cumulative log likelihood ratio at 2:03 as a function of position for environment 2/L:L. For each position, the figure shows the maximum cumulative log likelihood ratio for the 2/L:L environment over all velocity hypotheses for that position.

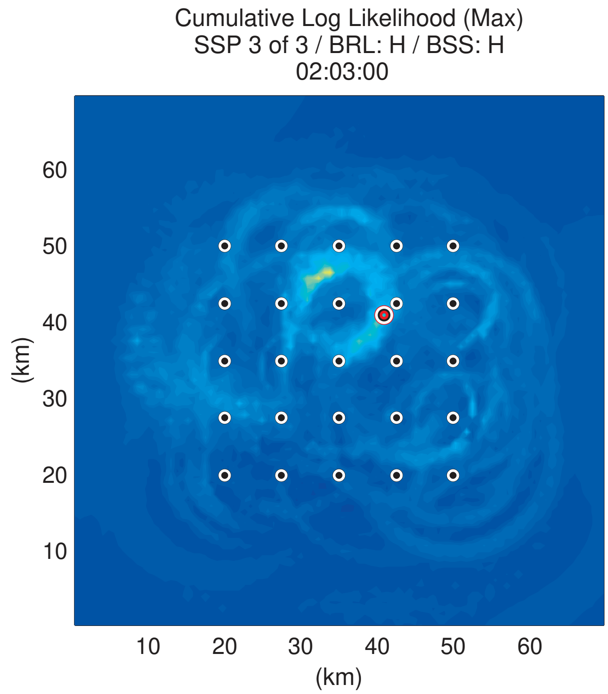

Figure 14. Maximum cumulative log likelihood ratio at 2:03 as a function of position for environment 3/H:H. For each position, the figure shows the maximum cumulative log likelihood ratio for the 3/H:H environment over all velocity hypotheses for that position.

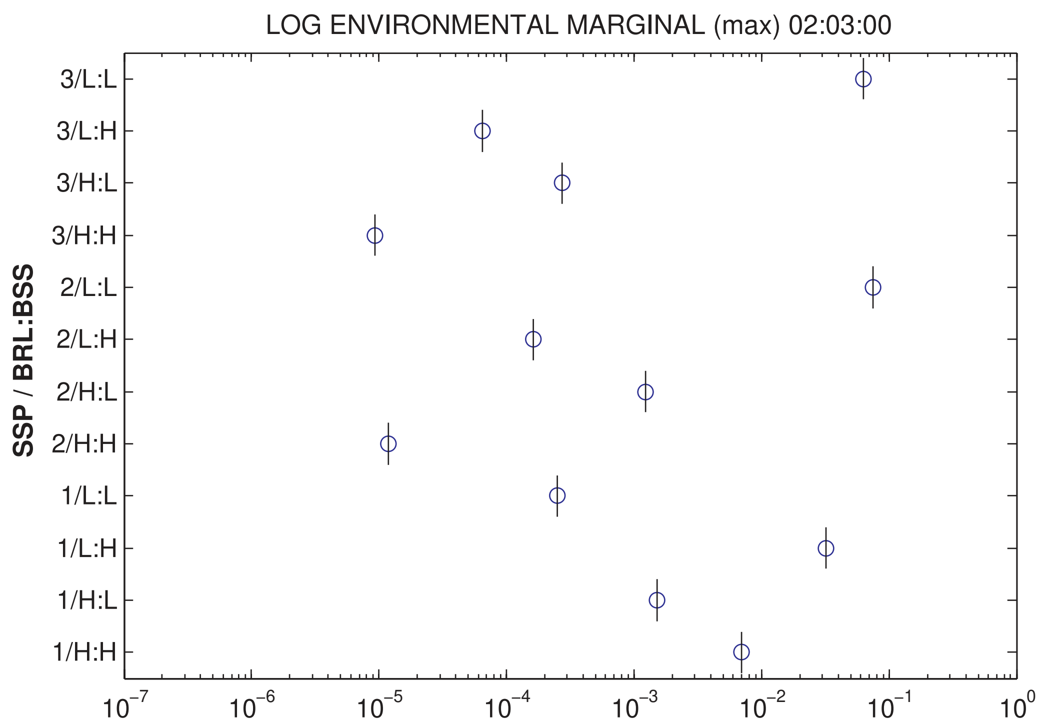

Figure 15. Maximum cumulative log likelihood ratio at time 2:03 as a function of environment. The figure shows the maximum cumulative log likelihood ratio over position and velocity for each of the environments.

VII. SUMMARY AND CONCLUSIONS

One of the major difficulties in using performance predictions in tactical decision aids such as trackers is that use of incorrect predictions can lead to results that are worse than using no predictions at all. The extension of LRT to include environmental uncertainty is a method of dealing with uncertain performance prediction. The example shows that incorporating the environmental uncertainty into LRT allowed us to gain track in a situation with substantial environmental uncertainty. We also showed that picking the wrong environment in this case can lead to failure to detect and track the target. These results indicate that quantifying environmental uncertainty and incorporating it into tactical decision aids such as LRT can provide a substantial benefit. In particular, it can mean the difference between being able to detect and track a target and not. In the future we hope to apply these techniques to real data to see if we can obtain improvement by incorporating performance prediction while maintaining robustness to environmental uncertainty.

VIII. ACKNOWLEDGMENTS

This work was sponsored by the Office of Naval Research under the "Capturing Uncertainty for the Common Tactical/Environmental Picture" program, the current sponsor of which is Dr. Douglas Abraham, ONR Code 321. Funding for METRON was under Contract N00014-00-D-0125. Funding for APL-UW was under Contract N00014-00-G-0460. Funding for NRL-SSC was under Contract N00014-04-WX-20583. Funding for ARL:UT was under Contract N00014-00-G-0450-02. We would like to thank Dr. Karl Fisher, for review of the manuscript, and Mr. Timothy Hawkins, for assistance in using BASIS.

IX REFERENCES

1. Oceanographic and Atmospheric Master Library (OAML) High Frequency Bottom Loss (HFBL), Version 2.2

2. H. C. Romesburg, *Cluster Analysis for Researchers* (Lifetime Learning Publications, Belmont, CA 1984).

3. J. H. Ward, "Hierarchical Grouping to Optimize an Objective Function" J. Am. Stat. Assoc., **58**, 236 – 244 (1963).

4. R. Keenan, "Software Design Description for the Comprehensive Acoustic System Simulation (CASS Version 3.0) with the Gaussian Ray Bundle Model (GRAB Version 2.0)," NUWC-NPT Technical Document 11231 1 June 2000.

5. R.J. Urick, *Principles of Underwater Sound*, (Peninsula Publishing, Los Altos, CA, 1984), 3rd ed.

6. R.E. Kell, "On the Derivation of Bistatic RCS from Monostatic Measurements," Proc. IEEE, **52**, 983–988 (1965).

7. R.L. Eigel, Jr., P.J. Collins, A.J. Terzuoli, Jr., G. Nesti, and J. Fortuny, "Bistatic Scattering Characterization of Complex Objects," IEEE Trans. Geoscience Remote Sensing, **38**, 2078-2092 (2000).

8. D. M. Drumheller, M. G. Hazen, and L. E. Gilroy "The Bistatic Acoustic Simple Integrated Structure (BASIS) Target Strength Model," NRL/FR-MM/7140--02-10,019, Naval Research Laboratory, Washington, DC, May 2002.

9. L. D. Stone, C. A. Barlow, and T. L. Corwin, *Bayesian Multiple Target Tracking* (Artech House, Boston, 1999).

10. L. D. Stone and Bryan R. Osborn, "Effect of Environmental Prediction Uncertainty on Target Detection and Tracking" in *Proceedings of Signal and Data Processing of Small Targets, SPIE conference on Defense and Security*, 12 – 16 April 2004, Orlando, FL, pp. 58 -69.

11. A. A. Ganse and D. R. Jackson, “"A Two-Layer Analytic Bottom Acoustic Model with Derivatives", APL-UW Technical Memorandum 5-05, Applied Physics Laboratory, University of Washington, August 2005.

12. SHAREM 134 and 138 NAVOCEANO processed Data and Pre and Post Exercise Report

13. P. H. Dahl, "ASIAEX East China Sea Cruise Report of Activities of the *R/V Melville*, 29 May to 9 June 2001," APL-UW Technical Memorandum TM 7-01, July 2001.